Journal of Alloys and Compounds 778 (2019) 618–624

Contents lists available at ScienceDirect

Journal of Alloys and Compounds

journal homepage: http://www.elsevier.com/locate/jalcom

Structural, thermal and magnetic properties of $Y_2Fe_2Si_2C$

R.A. Susilo [a, *], C.-H. Hsu [b, c], H. Lin [d], J.M. Cadogan [a], W.D. Hutchison [a], S.J. Campbell [a]

[a] School of Physical, Environmental and Mathematical Sciences, UNSW Canberra at the Australian Defence Force Academy, Canberra, BC, ACT 2610, Australia
[b] Centre for Advanced 2D Materials and Graphene Research Centre, National University of Singapore, 117546, Singapore
[c] Department of Physics, National University of Singapore, 117542, Singapore
[d] Institute of Physics, Academia Sinica, Taipei, 11529, Taiwan

ARTICLE INFO

Article history:
Received 11 September 2018
Received in revised form
22 October 2018
Accepted 1 November 2018
Available online 16 November 2018

Keywords:
Rare-earth intermetallics
Mössbauer spectroscopy
Specific heat
Lattice thermal expansion

ABSTRACT

We report detailed investigations on the structural, thermal and magnetic properties of $Y_2Fe_2Si_2C$ over the temperature range 2–300 K using x-ray diffraction, specific heat, ^{57}Fe Mössbauer spectroscopy and first-principles calculations. Low temperature measurements show no pronounced anomalies which might signal magnetic ordering of the Fe sublattice at low temperature. Analyses of the specific heat data of $Y_2Fe_2Si_2C$ reveal the presence of a localised Einstein mode, suggesting the importance of an optical contribution to the phonon spectrum of $Y_2Fe_2Si_2C$. Based on electronic structure calculations, we found a low density of states of the Fe 3*d* bands at the Fermi level. The corresponding density of states are below the Stoner criterion, thus indicating a non-magnetic state of the Fe atoms in $Y_2Fe_2Si_2C$, in agreement with the experimental findings.

1. Introduction

$R_2Fe_2Si_2C$ (Y, La - Nd, Sm, Gd - Tm and Lu) compounds crystallise in the monoclinic $Dy_2Fe_2Si_2C$-type structure with the *C*2/*m* space-group [1–3]. The R, Fe and Si atoms occupy the 4*i* sites (*m* point symmetry) in the unit cell with four atomic positions: $(x,0,z)$, $\left(x+\frac{1}{2},\frac{1}{2},z\right)$, $(-x,0,-z)$, and $\left(-x+\frac{1}{2},\frac{1}{2},-z\right)$, while the C atom occupies the 2*a* site (*2/m* point symmetry) with two atomic positions: $(0,0,0)$ and $\left(\frac{1}{2},\frac{1}{2},0\right)$. The magnetic studies of the $R_2Fe_2Si_2C$ (R = Y, Pr, Nd, Gd, Tb, Dy, Ho and Er) compounds by Schmitt et al. [4] and Pöttgen et al. [2] revealed that the magnetism of the $R_2Fe_2Si_2C$ (R = Nd, Gd, Tb, Dy, Ho, Er and Tm) set of compounds can be attributed solely to the R atoms, *i.e.* the Fe atom was reported to be non-magnetic as indicated by the similarity between the values of the experimental effective moment and the theoretical effective moment for the R^{3+} ions. However, neutron diffraction studies on $Nd_2Fe_2Si_2C$ and $Tb_2Fe_2Si_2C$ were interpreted in terms of the magnetic ordering in both the R and Fe sublattice [5].

Recently, we used high-resolution neutron diffraction to determine the magnetic structures of $R_2Fe_2Si_2C$ (R = Gd, Tb, Dy and Ho) compounds [6–9]. The magnetic structures of the Gd, Tb and Ho compounds below their antiferromagnetic ordering temperatures of 39 K, 44 K and 16 K, respectively, are characterised by the propagation vector of $\mathbf{k} = [0, 0, \frac{1}{2}]$ with the rare-earth magnetic moments pointing along the *b*-axis. $Dy_2Fe_2Si_2C$ on the other hand is antiferromagnetic below the Néel temperature of $T_N \sim 26$ K and undergoes a spin-reorientation transition at the lower temperature of $T_t \sim 6$ K [9]. ^{57}Fe Mössbauer spectroscopy has been used to establish that the Fe is non-magnetic in $R_2Fe_2Si_2C$ (R = Gd, Tb, Dy and Ho). The increase in linewidth observed in the ^{57}Fe Mössbauer spectra obtained for the set of $R_2Fe_2Si_2C$ compounds below their antiferromagnetic ordering temperature T_N has been used to track the temperature dependence of the antiferromagnetic order of the R sublattice, with this behaviour indicating that the line broadening is related to a transferred hyperfine field at the Fe site due to the ordering of the R sublattice [6–9].

Previous magnetic studies revealed no magnetic phase transition in $Y_2Fe_2Si_2C$ down to 2 K [4], thus indicating that $Y_2Fe_2Si_2C$ acts as an ideal non-magnetic reference material for investigating the magnetism of the $R_2Fe_2Si_2C$ system. Accordingly, we have used $Y_2Fe_2Si_2C$ as a reference material to estimate the magnetic contribution to the total specific heat of magnetic $R_2Fe_2Si_2C$ compounds

* Corresponding author. Present address: Center for High Pressure Science and Technology Advanced Research, Shanghai, 201203, China.
E-mail address: resta.susilo@hotmail.com (R.A. Susilo).

https://doi.org/10.1016/j.jallcom.2018.11.010
0925-8388/

[7–10]. Despite the significance of $Y_2Fe_2Si_2C$ for enhanced understanding of the magnetism of $R_2Fe_2Si_2C$ compounds, no detailed studies have so far been reported for $Y_2Fe_2Si_2C$. In this paper, we have used X-ray diffraction, ^{57}Fe Mössbauer spectroscopy, specific heat measurements and first-principles calculations to investigate the structural, thermal and magnetic properties of $Y_2Fe_2Si_2C$. Our low temperature specific heat, X-ray diffraction and ^{57}Fe Mössbauer spectroscopy measurements reveal no pronounced anomalies, thus excluding the presence of any magnetic ordering of the Fe sublattice. First-principles calculations also confirm a non-magnetic state of $Y_2Fe_2Si_2C$. However, we found that it is necessary to consider the Debye-Einstein model to properly describe the specific heat data, highlighting the importance of the optical contributions to the phonon spectrum of $Y_2Fe_2Si_2C$.

2. Experimental methods

The polycrystalline $Y_2Fe_2Si_2C$ sample was prepared by arc melting the constituent elements of purity better than 99.9 wt% under a high purity argon atmosphere (< 1 ppm impurity), following the procedure outlined by Pöttgen et al. [2]. The appropriate quantities of Y metal, Fe powder, Si powder, and graphite flakes in a total amount of ~500 mg, were first cold-pressed together into a pellet. This pressed pellet was then melted in an argon arc furnace. To ensure homogeneity, the sample was turned and re-melted several times. In order to compensate for weight loss during the melting (typically around 2% weight loss), it was necessary to add an excess of 2% of yttrium before melting. The resulting ingot is grey with metallic lustre and stable in air for months. The ingot was then powdered in air.

X-ray powder diffraction (XRD) patterns were collected at various temperatures between 300 K and 20 K using a PANalytical Empyrean diffractometer (Cu-K_α radiation) equipped with an Oxford Instruments Phenix closed-cycle refrigerator. All XRD patterns were refined by the Rietveld method using the FullProf/Winplotr software [11,12]. For specific heat measurements, the $Y_2Fe_2Si_2C$ powder sample was pressed and cut into a square-shape around 3 mm × 3 mm. The specific heat data was measured using a Quantum Design Physical Property Measurement System (PPMS) from 2 K to 300 K.

^{57}Fe Mössbauer spectra of $Y_2Fe_2Si_2C$ were collected in standard transmission mode using a ^{57}Co-**Rh** source. The spectrometer was calibrated with an α-Fe foil at room temperature and the sample temperature was varied from 11 K to 293 K using a closed-cycle refrigerator. All spectra were fitted using the Recoil software [13].

Full-potential first-principles electronic structure calculations were performed with the linear augmented-plane-wave (LAPW) method using the WIEN2K package [14] within the framework of the density functional theory (DFT). The Perdew-Burke-Ernzerhof (PBE) functionals [15] under the generalized gradient approximation (GGA) were used to describe the exchange-correlation potential. Lattice parameters and atomic positions obtained from diffraction experiments were used as input parameters and no geometry optimisations were employed in the calculations.

3. Results

3.1. Crystal structure

The X-ray diffraction pattern of $Y_2Fe_2Si_2C$ obtained at 295 K is shown in Fig. 1. Refinement of the X-ray diffraction pattern confirmed the formation of the monoclinic $Dy_2Fe_2Si_2C$-type structure with an impurity phase identified as $YC_{0.33}$ (yttrium carbide) present in the amount of 2.8 wt%. The refinement parameters are

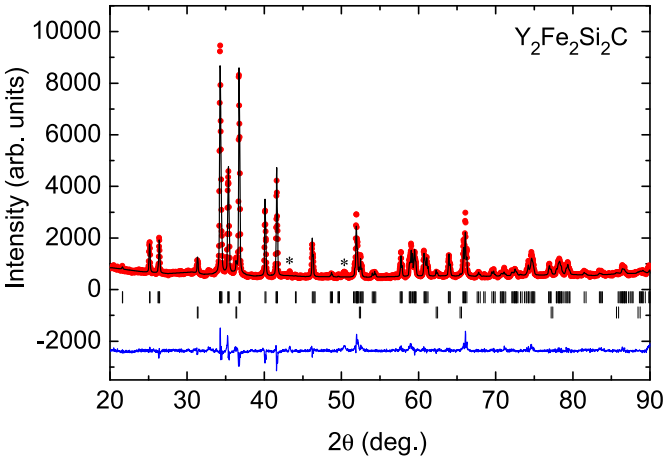

Fig. 1. Rietveld refinements of the X-ray diffraction pattern of $Y_2Fe_2Si_2C$ collected at 295 K (Cu-K_α radiation). The Bragg markers from top to bottom represent $Y_2Fe_2Si_2C$ and the impurity phase $YC_{0.33}$ (2.8 wt%), respectively with the differences between the experimental and calculated patterns shown by the blue line. The asterisks indicate peaks from an unknown impurity. (For interpretation of the references to colour in this figure legend, the reader is referred to the Web version of this article.)

presented in Table 1. We explored the possibility of off-stoichiometric samples due, for example, to weight losses on arc melting, by allowing the atomic occupations to vary in our set of refinements. In the event, such variations to the atomic occupations led to refinements with higher R_{Bragg} and R_F values than those obtained using ideal occupancies. The values for the ideal occupancies were therefore applied in the final refinements.

3.2. Specific heat

Previous magnetic studies show that $Y_2Fe_2Si_2C$ does not order magnetically down to 2 K [4]. Similarly, our zero field specific heat study on $Y_2Fe_2Si_2C$ (Fig. 2(a)) shows no anomalies down to 2 K. In the low temperature region ($T < 70$ K) the C_P/T versus T^2 curve is linear and can be fitted with $C_p(T) = \gamma T + \beta T^3$ (inset of Fig. 2(a)), yielding the Sommerfeld coefficient, $\gamma = 16.3(5)$ mJ/mol.K^2 and the β value of 0.133(1) mJ/mol.K^4. The Debye temperature θ_D calculated from the β value is 468(1) K. The C_P data of $Y_2Fe_2Si_2C$ over the temperature range of measurement were then fitted using the Debye model *i.e.* $C_p = \gamma T + 9NR\left(\frac{T}{\theta_D}\right)^3 \int_0^{\frac{\theta_D}{T}} \frac{x^4 e^x}{(e^x-1)^2} dx$ (where N is the number of atoms per formula unit). During the fitting process, γ was kept constant at 16.3 mJ/mol.K as determined above. The θ_D obtained from the least-squares fitting to the $C_p(T)$ data is 490(2) K, slightly larger than the value of 468 K derived from fitting the low temperature $C_p(T)$ data. The best fit curve to the $C_p(T)$ data using the Debye model is plotted as the dashed line in Fig. 2(a).

It can be seen that fitting the $C_p(T)$ curve using the Debye model

Table 1
Crystallographic data for $Y_2Fe_2Si_2C$ ($C2/m$ space group) as determined by x-ray powder diffraction at room temperature. (see Fig. 1).

Atom	x	y	z
Y	0.5616(11)	0	0.294(2)
Fe	0.205(2)	0	0.097(3)
Si	0.156(3)	0	0.700(3)
C	0	0	0
$a = 10.615(15)$ Å	$b = 3.9234(6)$ Å	$c = 6.7489(9)$ Å	$\beta = 129.27(1)^\circ$
	$R_{Bragg}(\%) = 12.9$	$R_F(\%) = 10.6$	

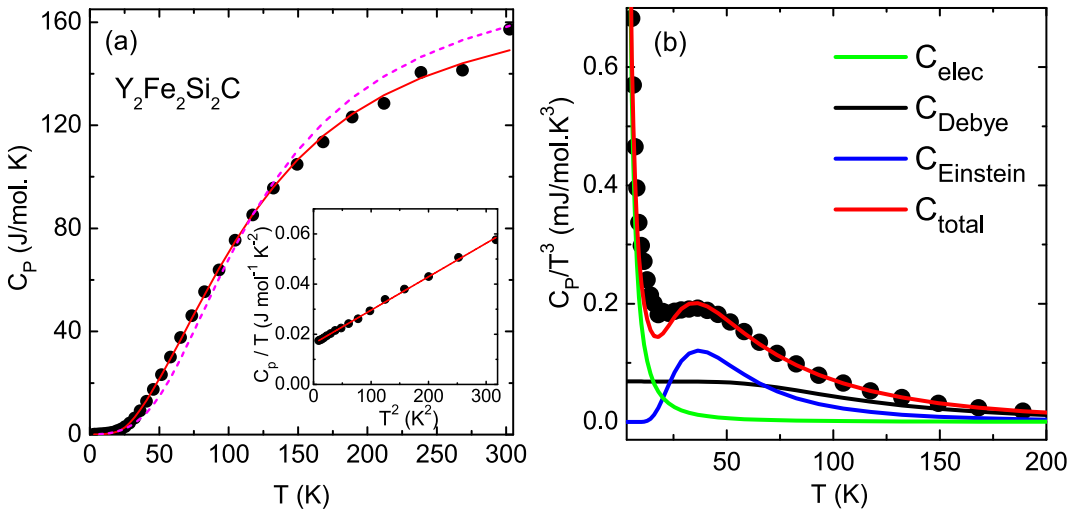

Fig. 2. (a) Zero field specific heat of $Y_2Fe_2Si_2C$. The dashed line represents a fit to the data (closed circles) with the Debye model while the solid line is a fit using the Debye-Einstein model as discussed in the text. The inset shows the low temperature C_P/T vs T^2 plot. (b) A graph of C_P/T^3 versus T for $Y_2Fe_2Si_2C$. The red line shows the fit obtained from the Debye-Einstein model (Eq. (1)), with the individual components as described in the text. (For interpretation of the references to colour in this figure legend, the reader is referred to the Web version of this article.)

resulted in a poor fit as evident by the deviation of the fitted curve from the experimental data above ~30 K. This deviation might be due to the importance of the optical contributions (Einstein term) to the phonon spectrum of $Y_2Fe_2Si_2C$ which is highlighted by the presence of a hump in the C_P/T^3 versus T curve at $T \sim 50$ K (see Fig. 2(b)). In order to describe fully the experimental C_P data we have employed both the Debye and Einstein models which can be written as

$$C_p = \gamma T + 9Rn_D\left(\frac{T}{\theta_D}\right)^3 \int_0^{\frac{\theta_D}{T}} \frac{x^4 e^x}{(e^x-1)^2}dx + 3Rn_E \frac{x_E^2 \exp(x_E)}{(\exp(x_E)-1)^2}. \quad (1)$$

The first term represents the electronic contribution to the specific heat whereas the second and the third terms represent the Debye and Einstein terms, respectively, with $x_E = \theta_E/T$ where θ_E is the Einstein temperature. n_D and n_E are the number of the Debye and Einstein modes, respectively, whose sum should be equal to the number of atoms per formula unit.

In Table 2, we present the fitting parameters to the specific heat data of $Y_2Fe_2Si_2C$ using the Debye-Einstein model as in Eq. (1). The data were well described with the Debye temperature of $\theta_D = 572(12)$ K and the Einstein temperature of $\theta_E = 184(3)$ K. The Debye temperature obtained from the Debye-Einstein model is higher than that obtained from the Debye model. This is expected since the Debye temperature derived from the Debye model represents the whole phonon spectrum (both the acoustic and optic modes), whereas the Debye temperature in the Debye-Einstein model represents the acoustic modes only. The sum of n_D and n_E is 6.7 close to that expected in the case of $R_2Fe_2Si_2C$ where $n_D + n_E = 7$. As is evident from the C_P/T^3 versus T curve shown in Fig. 2(b), the hump in the specific heat data around $T \sim 50$ K is reproduced well by the Einstein modes represented in our fit, reflecting the importance of the optical contribution (Einstein term) to the phonon spectrum of $Y_2Fe_2Si_2C$.

Table 2
Fitted parameters to the specific heat data of $Y_2Fe_2Si_2C$ (see Fig. 2).

Parameters	Debye model	Debye-Einstein model
γ (mJ/mol K^2)	16.3(5)	16.3 (fixed)
β (mJ/mol K^4)	0.133(1)	–
θ_D (K) (low T)	468(1)	–
θ_D (K)	490(2)	572(12)
n_D	–	5.1(1)
θ_E (K)	–	184(3)
n_E	–	1.6(2)

3.3. Thermal expansion

The temperature dependences of the lattice parameters and the unit cell volume of $Y_2Fe_2Si_2C$ from 20 K to 300 K are shown in Fig. 3. The lattice parameters and the unit cell volume of $Y_2Fe_2Si_2C$ decrease monotonically from 300 K down to 20 K. In order to describe the volume and linear thermal expansion curves, we first used the Grüneisen approximation for the zero pressure equation of state in which the effects of thermal expansion are considered as elastic strains [16]. Within the first-order Grüneisen approximation, the temperature dependence of the unit cell volume can be expressed as

$$V(T) = V_0 + x_V U(T) \quad (2)$$

where V_0 is the unit cell volume at 0 K and $x_V = \frac{\gamma_g}{B_0}$, γ_g is a Grüneisen parameter and B_0 the isothermal bulk modulus. $U(T)$ is the internal energy of the system which can be written (within the Debye model) as

$$U(T) = 9Nk_BT\left(\frac{T}{\theta_D}\right)^3 \int_0^{\frac{\theta_D}{T}} \frac{x^3}{e^x-1}dx \quad (3)$$

where N is the number of atoms in the unit cell ($N = 14$ in the case of $R_2Fe_2Si_2C$), k_B is the Boltzmann constant and θ_D is the Debye temperature. A similar expression can also be applied to the temperature dependence of the individual lattice parameters which

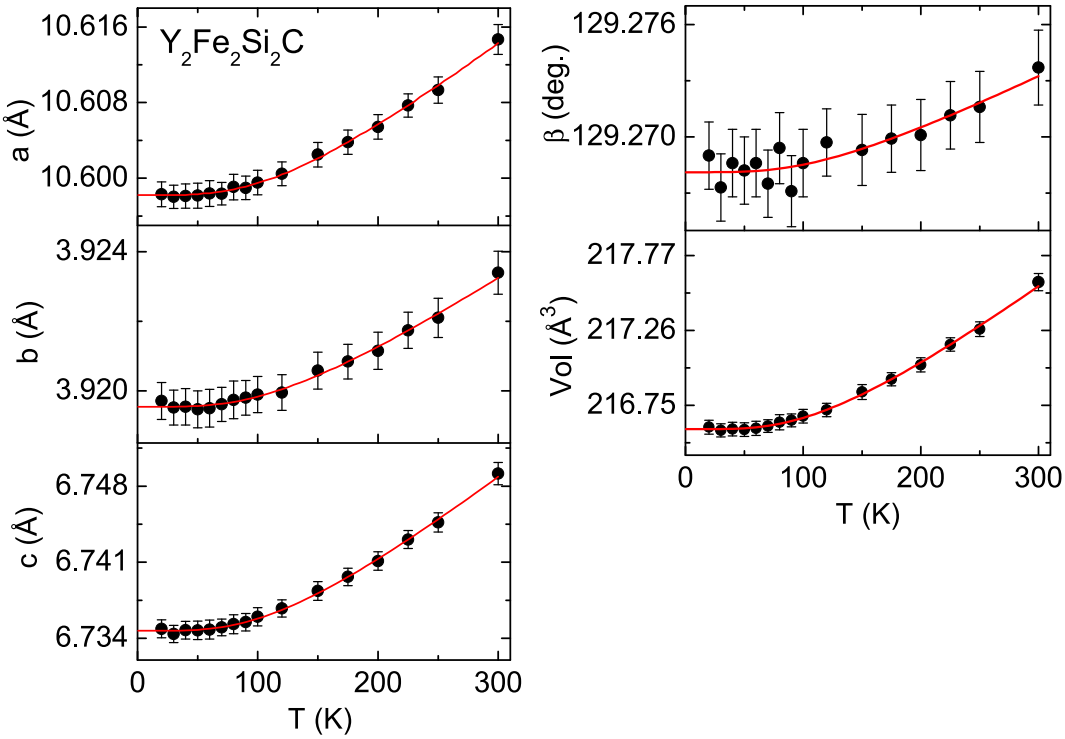

Fig. 3. Temperature dependence of the lattice parameters and the unit cell volume of $Y_2Fe_2Si_2C$. The solid lines represent fits to the experimental data (closed circles) using the Debye model and extrapolated to $T = 0$ K.

takes the form

$$l(T) = l_0 + x_l U(T) \tag{4}$$

where l represents the lattice parameters (a, b, c and β), l_0 represents the lattice parameters at 0 K (temperature independent term) and x_l is a constant of proportionality.

The solid lines in Fig. 3 represent the fits obtained to the data using Eqs. (2) and (4). The fits highlight that no deviation of the temperature dependence of the lattice parameters and the unit cell volume from the Debye model is observed down to 20 K. By comparison the temperature dependence of the lattice parameters and the unit cell volume of $Tb_2Fe_2Si_2C$ show a strong deviation from the Debye model due to the presence of spontaneous magnetostriction related to the ordering of the Tb magnetic sublattice [8]. The least-squares fitting procedure to the temperature dependence of the unit cell volume yields the Debye temperature of $\theta_D = 501(16)$ K. The fitted constant γ_g/B_0 is 0.11(2) GPa^{-1} which is comparable to the value determined for FeSi *i.e.* 0.14(1) GPa^{-1} [17]. Since the Grüneisen parameter γ_g is unknown, the related Bulk modulus B_0 of $Y_2Fe_2Si_2C$ cannot be determined in this work. The fitted parameters obtained from the unit cell volume and the lattice parameters of $Y_2Fe_2Si_2C$ using the Debye model are summarised in Table 3. Note that due to a large uncertainty in the β parameter, the Debye temperature determined from the unit cell volume was kept constant during the fitting of the β parameter.

Although the temperature dependence of the lattice parameters and the unit cell volume can be described by the Debye model, our analysis in Section 3.2 revealed that a localised Einstein mode is needed to describe the specific heat data of $Y_2Fe_2Si_2C$. Correspondingly, we therefore expect that the thermal expansion data would also reflect the presence of an Einstein mode.

In order to investigate the presence of an Einstein mode, we re-evaluated the temperature dependence of the unit cell volume of $Y_2Fe_2Si_2C$ using the Debye-Einstein model. Within the Debye-Einstein model, the temperature dependence of the unit cell volume should be modified by introducing an additional term as follows (e.g. Ref. [18])

Table 3
Fitted parameters of the lattice and volume thermal expansion of $Y_2Fe_2Si_2C$ obtained using Eqs. (2) and (4).

	V_0 (Å^3), l_0 (Å)	x_l ($\times 10^{-2}$ GPa^{-1})	θ_D (K)
V (Å^3)	216.59(2)	11(2)	501(16)
a (Å)	10.5981(5)	0.18(5)	481(25)
b (Å)	3.9195(2)	0.04(2)	529(48)
c (Å)	6.7347(3)	0.16(3)	481(19)
β (°)	129.268(2)	0.06(5)	501 (fixed)

$$V(T) = V_0 + x_V U(T) + x_E E(T) \tag{5}$$

where x_V and x_E are constants of proportionality. $U(T)$ is calculated using the Debye model as in Eq. (3) whereas $E(T)$ represents the internal energy of an Einstein oscillator which can be expressed as

$$E(T) = \frac{3Nk_B\theta_E}{(\exp(\theta_E/T) - 1)}. \tag{6}$$

The parameters determined from fits to the temperature dependence of the unit cell volume of $Y_2Fe_2Si_2C$ using both the Debye and Debye-Einstein models are summarised in Table 4. As noted (Fig. 3), the Debye model describes the data well with the Debye-Einstein model also giving a very good representation of the experimental data. The fitted curve derived using the Debye-Einstein model is virtually indistinguishable from the Debye model, although the least-square fitting indicates that the fitting to the unit cell volume using the Debye-Einstein model as in Eq. (5) yields a smaller χ^2 value compared with the Debye model only

Table 4
Comparison of the fitted parameters to the lattice and volume parameters of $Y_2Fe_2Si_2C$ obtained using the Debye and Debye-Einstein models.

Parameters	Debye model	Debye-Einstein model
V_0 (Å^3)	216.59(2)	216.58(3)
θ_D (K)	501(16)	578(26)
θ_E (K)	–	166(79)
x_V	0.11(2)	0.10(4)
x_E	–	0.02(2)
χ^2	0.97	0.85

(see Table 4), thus indicating that the Debye-Einstein model is more appropriate to describe the temperature dependence of the unit cell volume of $Y_2Fe_2Si_2C$. In addition, the Debye and Einstein temperatures determined from the fit to the unit cell volume, *i.e.* θ_D of 578(26) K and θ_E = 166(79) K, agree with those obtained from the fit to the specific heat data (θ_D = 572(12) K and θ_E = 184(3) K; Table 2).

3.4. ^{57}Fe Mössbauer spectroscopy

The ^{57}Fe Mössbauer spectra of $Y_2Fe_2Si_2C$ obtained at various temperatures from 300 K to 11.4 K show no evidence of magnetic splitting confirming that the Fe is non-magnetic in this compound. Examples of these spectra for 293 K and 11.4 K are shown in Fig. 4. All spectra can be fitted with a single doublet.

The temperature dependences of the hyperfine parameters for $Y_2Fe_2Si_2C$ are shown in Fig. 5. The linewidth is essentially temperature independent as evident from the absence of systematic line broadening down to 11 K (see Fig. 5(a)). By comparison, a small degree of spectral line broadening was observed in the ^{57}Fe Mössbauer spectra of $Gd_2Fe_2Si_2C$ [7], $Tb_2Fe_2Si_2C$ [8], $Dy_2Fe_2Si_2C$ [9] and $Ho_2Fe_2Si_2C$ [6] collected below the magnetic ordering temperatures with the line broadening associated with a small transferred hyperfine field at the Fe site due to the ordering of the surrounding R moments.

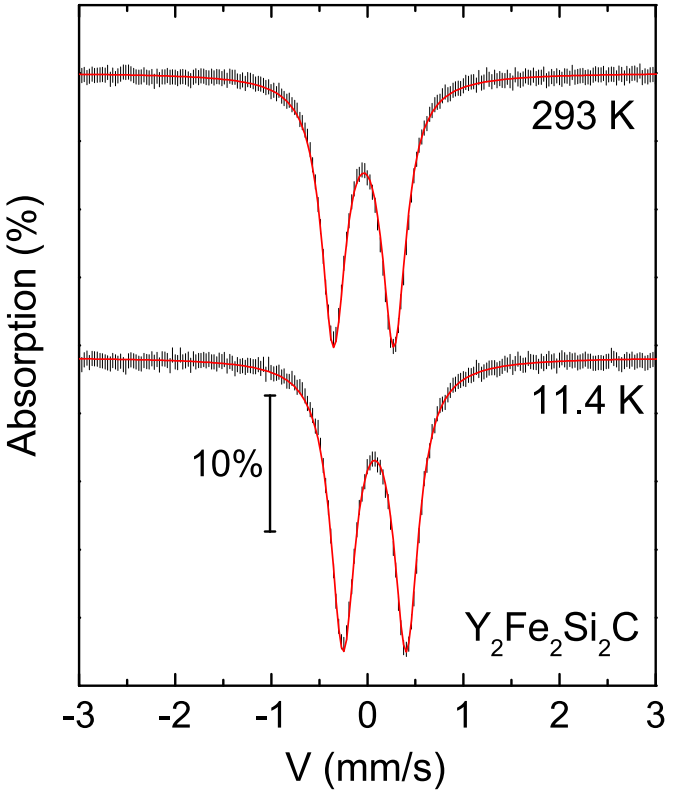

Fig. 4. ^{57}Fe Mössbauer spectra of $Y_2Fe_2Si_2C$ collected at 293 K and 11.4 K. The spectral fits are described in the text.

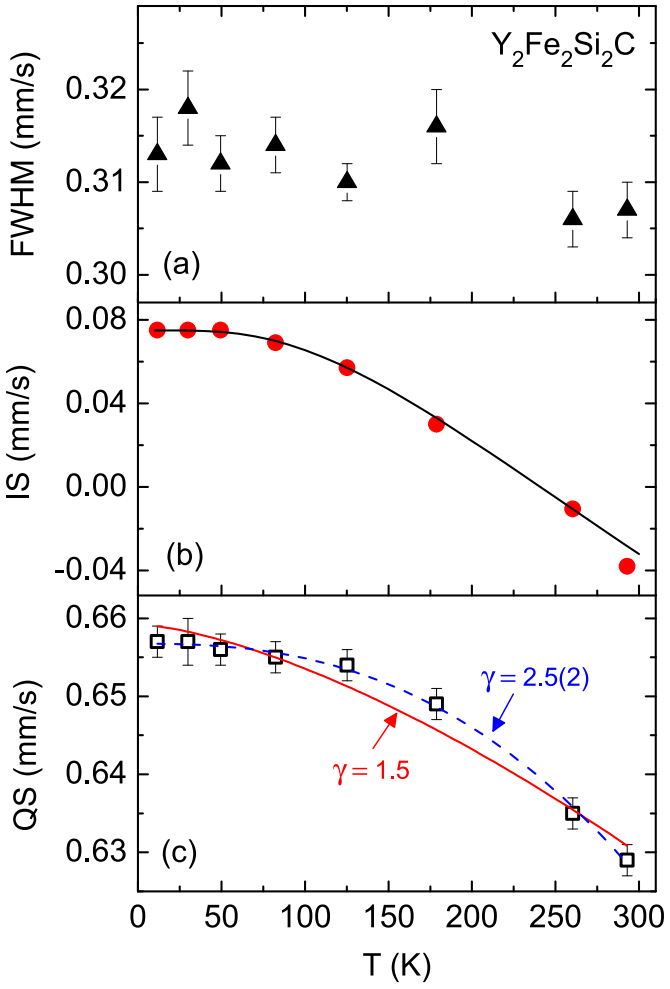

Fig. 5. Temperature dependence of (a) linewidth, (b) isomer shift (IS) and (c) quadrupole splitting (QS) of $Y_2Fe_2Si_2C$. The IS values are quoted relative to the α-Fe calibration. The solid line in (b) represents a fit with the second-order Doppler shift. The solid and dotted lines in (c) represent fits using Eq. (8) as described in the text.

As shown in Fig. 5(b), the isomer shift of $Y_2Fe_2Si_2C$ increases with decreasing temperature. The temperature dependence of the isomer shift is due to the second-order Doppler shift and can be described by the Debye model [19] *i.e.*

$$IS(T) = IS(0) - \frac{9}{2}\frac{k_B T}{Mc}\left(\frac{T}{\theta_M}\right)^3 \int_0^{\frac{\theta_M}{T}} \frac{x^3}{e^x - 1} dx, \qquad (7)$$

where c is the speed of light, M is the mass of the ^{57}Fe nucleus, θ_M is the Mössbauer Debye temperature and $IS(0)$ is the temperature-independent term of the isomer shift. The temperature dependence of the isomer shift of $Y_2Fe_2Si_2C$ can be fitted with θ_M = 475(7) K, which is slightly higher than the Debye temperature evaluated from the low temperature specific heat measurements, *i.e.* θ_D = 468 K. While these values agree within uncertainties, the difference is likely to be due to the fact that the Mössbauer Debye temperature represents the phonon spectrum due to the vibration

of the Fe atom whereas the Debye temperature estimated from the specific heat measurements reflects the overall phonon spectrum in the sample.

The temperature dependence of the quadrupole splitting (QS) of $Y_2Fe_2Si_2C$ also increases as the temperature is lowered. Following Verma and Rao [20], we fitted the temperature dependence of QS using

$$QS(T) = QS(0)(1 - bT^{\gamma}), \quad (8)$$

where $QS(0)$ is the quadrupole splitting at 0 K (temperature independent term) and b is the constant of proportionality. The temperature dependence of the QS was fitted initially by fixing the exponent γ to 1.5 with the resultant fitted curve plotted as a solid line in Fig. 5(c). This dependency-known as the $T^{3/2}$ law-has been observed in many metallic systems with non-cubic symmetry [21,22]. The $T^{3/2}$ law can account for the increase in QS upon lowering the temperature, however some deviation is clearly seen in the intermediate temperature region e.g. between ~100 K and ~200 K. We therefore allowed the exponent γ to vary, yielding $\gamma = 2.5(2)$ with the fitted curve shown as a dotted line in Fig. 5(c). The fitted curve with $\gamma = 2.5$ is clearly superior to the fitted curve obtained with the $T^{3/2}$ law, although the reason for this deviation from the 'universal' $T^{3/2}$ law is unknown at present. However it should be noted that such deviations from the $T^{3/2}$ law were observed in several cases involving transition metals and rare-earth metals hosts [20]. This deviation was also observed in the case of filled skutterudites $Eu_{0.88}Fe_4Sb_{12}$, where the temperature dependence of QS obtained from ^{57}Fe Mössbauer experiments can be well-fitted with $\gamma = 2.43$ [23].

3.5. Electronic density of states

The density of states (DOS) of $Y_2Fe_2Si_2C$ is presented in Fig. 6. The total DOS curve is characterised by a broad valence band from −5 eV to 2 eV relative to the Fermi energy (E_F) which is dominated by the Fe 3*d* states. The Fe 3*d* states are distributed from −5 eV to 2 eV forming a broad maximum centred at about −1 eV below E_F with a second maximum occurring around 1 eV above E_F. The Si 3*p* states are situated from −3 eV to −1 eV while the C 2*p* states are mainly distributed in the energy range −5 eV to −2 eV. The main contribution to the DOS at E_F originates primarily from the Fe 3*d* states with some admixture of the Y 5*d* and C 2*p* states, while the unoccupied states above 2 eV have a dominant contribution from the Y 5*d* states and minor contributions from the Fe 3*d* and C 2*p* states.

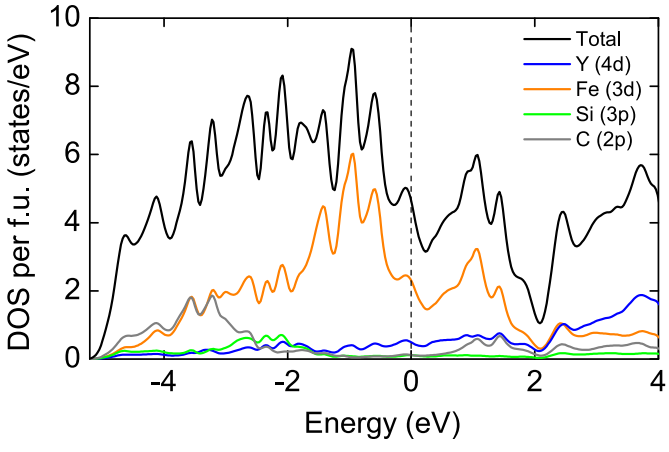

Fig. 6. Calculated total and partial density of states (DOS) of $Y_2Fe_2Si_2C$ per formula unit. The vertical dashed line indicates the Fermi energy (E_F).

The important feature of the DOS curve is the presence of strong hybridisation between the Fe 3*d*, Si 3*p* and C 2*p* states in the energy range between −5 eV to −1 eV. This $p-d$ hybridisation is also observed in the electronic structure calculations on other R-Fe-based compounds where the Fe atom bears no magnetic moment, such as in the R-FeSi [24–26], RFe_2Si_2 [27–29] and $R_2Fe_3Si_5$ [30] systems. We suggest that the strong hybridisation between the Fe 3*d* and C 2*p* states causes the increase of bandwidth of Fe 3d states. An example showing the effect of the strong $p-d$ hybridisation in reducing the magnetism of the 3*d* element is the disappearance of the Cr magnetic moment in RCr_2Si_2C [31]. First-principles calculations on YCr_2Si_2C reveal that the Cr magnetic moment in YCr_2Si_2 is gradually suppressed upon insertion of carbon [31] highlighting the importance of $p-d$ hybridisation in suppressing the magnetism of the transition metal in such compounds.

The density of states of the Fe 3*d* bands at E_F is only 2.3 states/eV per formula unit or 1.1 states/eV per Fe atom. Using a typical Stoner factor I for Fe of 0.46 eV [32], this value leads to $N(E_F)I = 0.51$ which is far below the Stoner criterion for ferromagnetism *i.e.* $N(E_F)I > 1$. This indicates that the $Y_2Fe_2Si_2C$ compound is far from being magnetic. This result is supported by the spin-polarised calculations on $Y_2Fe_2Si_2C$ (not shown here) which converge into a non-magnetic ground state as evidenced by the absence of the Fe band splitting.

The density of states at E_F ($N(E_F)$) of 4.7 states/eV per formula unit corresponds to a Sommerfeld coefficient of $\gamma_{band} = 11.1$ mJ/mol K^2, which is lower than the experimental γ_{exp} value of 16.3 mJ/mol K^2 as determined from the specific heat measurement. The mass enhancement factor λ, defined as $\gamma_{exp} = (1+\lambda)\gamma_{band}$, can be used to estimate the strength of the electron-electron and electron-phonon couplings. Based on the values of γ_{band} and γ_{exp} of 11.1 mJ/mol K^2 and 16.3 mJ/mol K^2, respectively, the enhancement factor λ is calculated to be 0.45, corresponding to weak electron-electron and electron-phonon interactions in $Y_2Fe_2Si_2C$.

4. Discussion

Analyses of the specific heat data and volume thermal expansion of $Y_2Fe_2Si_2C$ reveal the presence of a localised Einstein mode with $\theta_E = 180$ K corresponding to the energy of ~16 meV. The presence of an Einstein mode in $Y_2Fe_2Si_2C$ is rather unexpected. In general, the presence of a localised Einstein mode occurs in the systems with specific structure, *i.e.* cage-like structure such as in clathrates (e.g. Refs. [33,34]) and skutterudites (e.g. Refs. [35,36]) in which the Einstein mode is associated with the local vibration of the atoms inside the cage structure. In the case of $Y_2Fe_2Si_2C$, the presence of a cage structure in which the atoms are weakly bound is not obvious. Clearly, additional first-principles calculations to determine the phonon density of states of $Y_2Fe_2Si_2C$ would be beneficial to determine the origin of this Einstein mode. Further experimental investigations, such as inelastic neutron scattering, would also provide additional insights into the phonon spectrum of $Y_2Fe_2Si_2C$.

The first-principles calculations on $Y_2Fe_2Si_2C$ shown in Fig. 6 reveal that the Fermi level is located in a low DOS region of the Fe 3*d* bands. As a consequence, the Stoner criterion is not fulfilled in any case, and as such, is likely to account for the absence of the Fe sublattice ordering in the $R_2Fe_2Si_2C$ compounds. However, this will in fact change if the Fermi level is located at the peak of the Fe 3*d* bands (*i.e.* at ~ −1 eV), which will create an Fe moment instability and fulfilment of the Stoner criterion. It is known that by introducing an impurity with a different number of d-electrons into the

system, the Fermi level can be tuned to higher or lower energies. This creates the possibility of tuning the Fe 3d state to be close to magnetic, as in the case of R(Co, Ni)$_2$ [37] or R(Co, Ti)$_2$ [38]. Therefore, it would be interesting to study the evolution of the magnetism of the Fe sublattice in $R_2Fe_2Si_2C$ by decreasing the number of Fe-d electrons *i.e.* by partially substituting of the Fe atom with an element that has fewer d-electrons such as Re, Mn or Ti.

5. Conclusions

We have investigated the structural, thermal and magnetic properties of $Y_2Fe_2Si_2C$. From the ^{57}Fe Mössbauer spectroscopy measurements, we observed no systematic line broadening and anomalies in the quadrupole splitting in $Y_2Fe_2Si_2C$ down to ~11 K, thus excluding the presence of magnetic ordering of the Fe sublattice at low temperature. Similarly, specific heat and X-ray diffraction experiments show no pronounced anomalies at low temperatures which would signal magnetic ordering. In addition, we found the presence of a localised Einstein mode from the analyses of specific heat data which reflects the importance of optical contributions to the phonon spectrum of $Y_2Fe_2Si_2C$. We have shown that the density of states of the Fe 3*d* bands at the Fermi energy are below the Stoner criterion, thus accounting for the absence of Fe magnetism in $Y_2Fe_2Si_2C$.

Acknowledgments

RAS acknowledges a Research Publication Fellowship from UNSW Canberra.

References

[1] L. Paccard, D. Paccard, J. Less Common Met. 136 (1988) 297–301.
[2] R. Pöttgen, T. Ebel, C.B.H. Evers, W. Jeitschko, J. Solid State Chem. 114 (1995) 66–72.
[3] T. Hüfken, A.M. Witte, W. Jeitschko, J. Alloys Compd. 266 (1998) 158–163.
[4] D. Schmitt, D. Paccard, L. Paccard, Solid State Commun. 84 (1992) 357–361.
[5] J. Le Roy, D. Paccard, C. Bertrand, J.L. Soubeyroux, J. Bouillot, L. Paccard, D. Schmitt, Solid State Commun. 86 (1993) 675–678.
[6] R.A. Susilo, J.M. Cadogan, R. Cobas, W.D. Hutchison, M. Avdeev, S.J. Campbell, J. Appl. Phys. 117 (2015) 17C113.
[7] D.H. Ryan, N. Mas, R.A. Susilo, J.M. Cadogan, R. Flacau, J. Phys. Condens. Matter 27 (2015), 146005.
[8] R.A. Susilo, J.M. Cadogan, W.D. Hutchison, M. Avdeev, R. Cobas, S. Muñoz-Pérez, S.J. Campbell, J. Alloys Compd. 654 (2016) 392–398.
[9] R.A. Susilo, J.M. Cadogan, W.D. Hutchison, G.A. Stewart, M. Avdeev, S.J. Campbell, J. Phys. Condens. Matter 29 (2017), 115806.
[10] R.A. Susilo, J.M. Cadogan, W.D. Hutchison, S.J. Campbell, Phys. Status Solidi (A) 211 (2014) 1087–1091.
[11] J. Rodríguez-Carvajal, Physica B 192 (1993) 55–69.
[12] T. Roisnel, J. Rodríguez-Carvajal, Mater. Sci. Forum 378–381 (2001) 118–123.
[13] K. Lagarec, D.G. Rancourt, Recoil - Mössbauer Spectral Analysis Software for Windows, Ver. 1.0, Department of Physics, University of Ottawa, Ottawa, ON, Canada, 1998.
[14] P. Blaha, K. Schwarz, G. Madsen, D. Kvasnicka, J. Luitz, WIEN2K, An Augmented Plane Wave Plus Local Orbitals Program for Calculating Crystal Properties, 2001. Vienna University of Technology, Vienna.
[15] J.P. Perdew, K. Burke, M. Ernzerhof, Phys. Rev. Lett. 77 (1996) 3865.
[16] D. Wallace, Thermodynamics in Crystals, Dover, New York.
[17] L. Vočadlo, K.S. Knight, G.D. Price, I.G. Wood, Phys. Chem. Miner. 29 (2002) 132–139.
[18] A. Fortes, I. Wood, L. Vočadlo, H. Brand, K.S. Knight, J. Appl. Crystallogr. 40 (2007) 761–770.
[19] G.K. Shenoy, F.E. Wagner, G.M. Kalvius, G.K. Shenoy, in: F.E. Wagner (Ed.), Mössbauer Isomer Shifts, North-Holland Publishing Co., Amsterdam, 1978, pp. 49–110.
[20] H. Verma, G. Rao, Hyperfine Interact. 15 (1983) 207–210.
[21] E.N. Kaufmann, R.J. Vianden, Rev. Mod. Phys. 51 (1979) 161–214.
[22] R. Vianden, Hyperfine Interact. 15 (1983) 189–201.
[23] M. Reissner, E. Bauer, W. Steiner, P. Rogl, Hyperfine Interact. 158 (2004) 211–215.
[24] V. Klosek, J. Tobola, A. Vernière, S. Kaprzyk, B. Malaman, Eur. Phys. J. B 42 (2004) 219–230.
[25] X.B. Liu, Z. Altounian, J. Appl. Phys. 107 (2010) 09E103.
[26] P. Wlodarczyk, L. Hawelek, P. Zackiewicz, T.R. Roy, A. Chrobak, M. Kaminska, A. Kolano-Burian, J. Szade, Mater. Chem. Phys. 162 (2015) 273–278.
[27] M. Mihalik, J. Vejpravová, J. Rusz, M. Diviš, P. Svoboda, V. Sechovský, M. Mihalik, Phys. Rev. B 70 (2004) 134405.
[28] M. Mihalik, P. Svoboda, J. Rusz, M. Diviš, V. Sechovský, Physica B 367 (2005) 19–28.
[29] I. Hase, T. Yanagisawa, Physica C 471 (2011) 656–658.
[30] M. Winiarski, M. Samsel-Czekaa, Solid State Sci. 26 (2013) 134–138.
[31] V. Klosek, A. Vernière, B. Malaman, J. Tobola, S. Kaprzyk, Phys. Rev. B 78 (2008), 104419.
[32] J.F. Janak, Phys. Rev. B 16 (1977) 255–262.
[33] K. Suekuni, M.A. Avila, K. Umeo, H. Fukuoka, S. Yamanaka, T. Nakagawa, T. Takabatake, Phys. Rev. B 77 (2008), 235119.
[34] X. Zheng, S.Y. Rodriguez, L. Saribaev, J.H. Ross Jr., Phys. Rev. B 85 (2008), 214304.
[35] V. Keppens, D. Mandrus, B.C. Sales, B.C. Chakoumakos, P. Dai, R. Coldea, M.B. Maple, D.A. Gajewski, E.J. Freeman, S. Bennington, Nature 395 (1998) 876–878.
[36] R.P. Hermann, R. Jin, W. Schweika, F. Grandjean, D. Mandrus, B.C. Sales, G.J. Long, Phys. Rev. Lett. 90 (2003), 135505.
[37] M. Cyrot, M. Lavagna, J. Phys. 40 (1979) 763–771.
[38] C. Bonilla, D. Paudyal, J. Herrero-Albillos, V. Pecharsky, K. Gschneidner Jr., L. Garcia, F. Bartolomé, IEEE Trans. Magn. 50 (2014) 1–4.